



Influence of Tool Posture and Position on Stability in Milling with Parallel Kinematic Machine Tool

Muizuddin Azka^{1,2} · Keiji Yamada¹ · Mahfudz Al Huda² · Ryutaro Tanaka¹ · Katsuhiko Sekiya¹

Received: 24 March 2020 / Revised: 3 September 2020 / Accepted: 13 September 2020 / Published online: 15 October 2020
© Korean Society for Precision Engineering 2020

Abstract

This paper investigated the machining stability influenced by tool posture and position in ball-end milling with parallel kinematic machine tool (PKM). Initially, the geometric structure was identified, and the machinery stiffness was measured by impulse respond method at several positions with four tool postures. Then, the milling tests were conducted on flat work surface using a ball-end mills. Cutting force and acceleration signals of milling tests were measured by three-axis dynamometer and accelerometer. Furthermore, these signals were analyzed by using Fast-Fourier transform and Hilbert–Huang transform (HHT). The results showed that the length of arm change with tool posture, where the machinery stiffness decreased with the total length of arms for any tool position. The experimental results also demonstrated the machining stability varied with tool posture; the trend of stability corresponds with the machinery stiffness. The vibration analysis by HHT presented the increasing of power level in the time–frequency plot when the length of arm increase during milling process. Therefore, the geometric influence must be considered to support process planning on the PKM.

Keywords Tool posture and position · Ball-end milling · Parallel kinematic machine tool · Machinery stiffness · Machining stability · Hilbert–Huang transform

List of Symbols

a	Depth of slot (mm)
A_X	Acceleration signal in X -direction (m/s^2)
A_Y	Acceleration signal in Y -direction (m/s^2)
A_Z	Acceleration signal in Z -direction (m/s^2)
n	Spindle rotation (min^{-1})
f_n	Natural frequency (Hz)
f_T	Tooth-passing frequency (Hz)
f_c	Self-excited chatter frequency (Hz)
F_X	Force signal in X -direction (N)
F_Y	Force signal in Y -direction (N)
F_Z	Force signal in Z -direction (N)
G	Dynamic compliance ($\mu m/N$)
K	Machinery stiffness (MN/m)
N_f	Number of flutes
V_X	Feeding speed in X -direction (mm/min)

V_Y	Feeding speed in Y -direction (mm/min)
X	Machine coordinate system in X -axis (mm)
Y	Machine coordinate system in Y -axis (mm)
Z	Machine coordinate system in Z -axis (mm)
θ_A	Tool posture in A -axis ($^\circ$)
θ_B	Tool posture in B -axis ($^\circ$)

1 Introduction

A lot of mechanical parts contain complexed surfaces which are finished by ball-end of milling tool traveling along a desired cutting path. The tool axis is generally inclined against the machined surface for preventing the surface from touching the tool-tip center because of its low peripheral speed. Hence, five-axis machine tools are widely used for the machining in die and molds, aerospace, and automotive industries.

In those machining processes, in general, cutting conditions drastically change during the tool travels along the path. Therefore, many researchers discussed the machining stability in ball-end milling operations under different conditions. For example, Altintas et al. [1, 2] presented the stability in ball-end milling with different depth of cut and spindle

✉ Keiji Yamada
keiji@hiroshima-u.ac.jp

¹ Graduate School of Engineering, Hiroshima University, 1-4-1 Kagamiyama, Higashi-Hiroshima, Hiroshima 739-8527, Japan

² Agency for the Assessment and Application of Technology (BPPT), Jakarta 10340, Indonesia

speed. Shamoto et al. [3] predicted the influence of tool inclination on stability in ball-end milling. Matsumura et al. [4] discussed the stability in ball-end milling with changing the modal parameters of system. Selmi et al. [5] showed the influence of spindle position on stability. Authors also proposed an experimental method to analyze the change in stability during the end milling [6]. Those studies discussed the machining stability influenced by the directional cutting force coefficients and directional stiffness of cutting systems in serial machine tools.

In above previous works, classical serial Cartesian-design machining centers were used in both theoretical analysis and experiments, and it was shown that the mechanical stiffness of cutting system significantly affects the machining stability and the quality of machined surfaces. Alternatively, the parallel kinematic machine tool (PKM) has been introduced as a novel machine tool, where closed loop of parallel mechanism can realize high speed, high accuracy, and high rigidity theoretically [7–9]. This machine has high degree of freedom and can maneuver the cutting tool in 5-axis milling to accommodate the complex surface machining [10, 11]. However, it is not simple to achieve high speed cutting on the PKM, because it has relatively complex structure having six kinematic arms to control the posture and position of the spindle unit [12, 13]. So that, the homogeneous stiffness of machinery is not easily established over the whole working area on PKMs [14–16].

Therefore, in this paper, the influence of tool posture and position to the stability in milling process on parallel kinematic machine tool are evaluated in order to support process planning. We identify the geometric structure and measure the machinery stiffness of structure for different tool posture and position. Then, the milling tests are performed to analyze the machining stability with using two kinds of sensors.

2 Experimental Methods

2.1 Geometric Structure of Parallel Kinematic Machine

Figure 1 shows the structure of a parallel kinematic machine CNC milling (OKUMA, COSMO CENTER PM-600), which was used in this study. This machine has six arms supporting a spindle head on a platform. Each arm is connected to the base plate by a joint and to the platform by another spherical joint. And, a ball screw, a hollow servomotor and a rotary encoder are integrated within each arm [8]. Thus, position and posture of spindle are determined by the length of arms (distance between platform joints and base joints). It also noted that all dimensions in this figure correspond to ones for the machine origin.

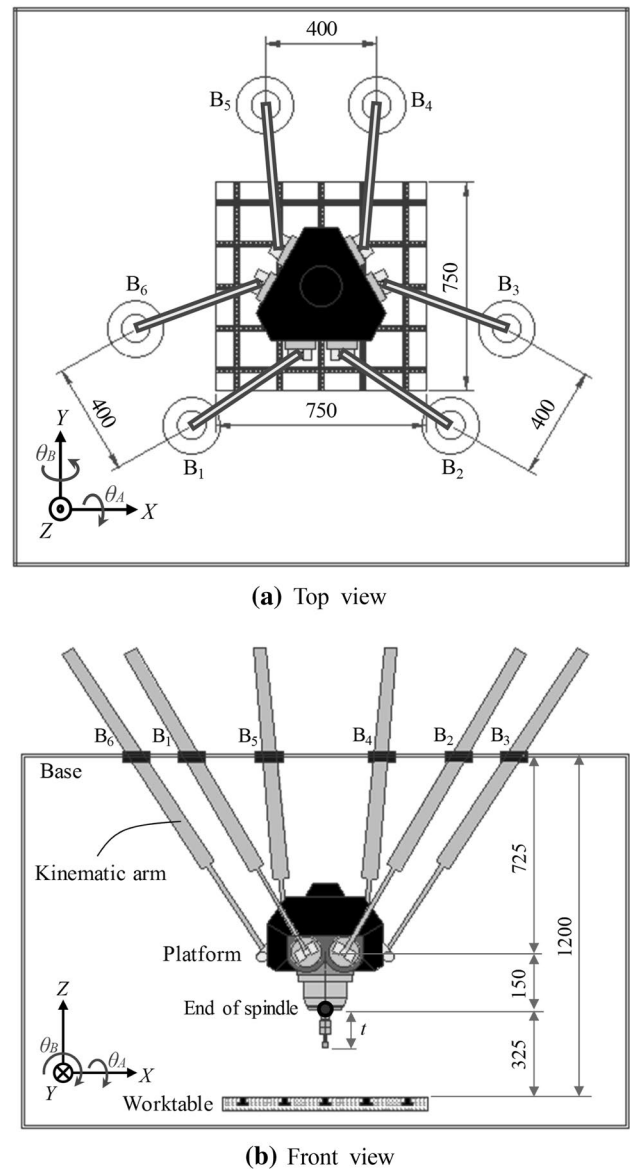


Fig. 1 Structure of parallel kinematic machine (machine origin)

Figure 2 shows geometry of a hexapod structure parallel kinematic machines. Lengths of the six arms l_1 – l_6 are calculated as

$$l_k = \left| \overrightarrow{B_k P_k} \right| \quad (k = 1, 2 \dots 6) \quad (1)$$

$$\overrightarrow{B_k P_k} = \overrightarrow{O P_0} + \overrightarrow{P_0 P_k} - \overrightarrow{O B_k} \quad (2)$$

where O is the global origin, P_0 is the center of platform, B_k and P_k represents joints on the base and the platform, respectively.

Vector $\overrightarrow{O B_k}$ is designed as shown in Fig. 1a and is constant for any positions and postures of tool. But, $\overrightarrow{P_0 P_k}$, a

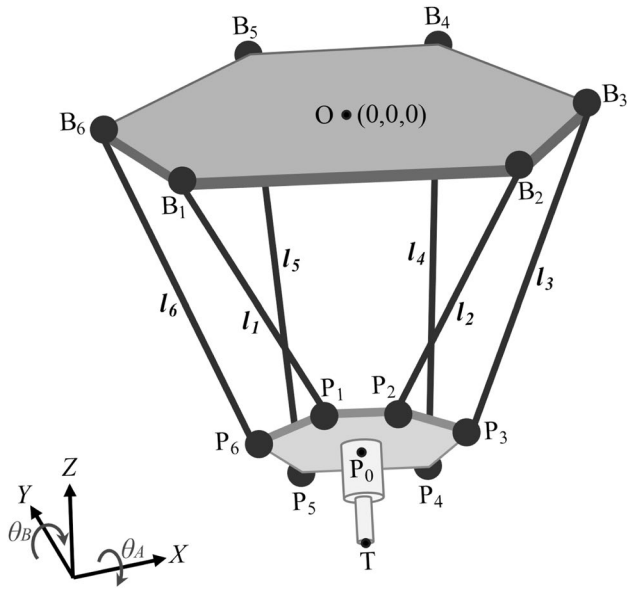


Fig. 2 Architecture of hexapod structure

vector from center to joint on the platform varies with the tool posture. The influence of tool posture can be expressed as rotations about X- and Y-axis as

$$\overline{P_0P_k} = R_X R_Y \overline{P_0P'_k} \tag{3}$$

where a vector \$\overline{P_0P'_k}\$ shows the original position of a platform joint with respect to the platform center (in Fig. 1). And, the rotation matrixes are

$$R_X = \begin{pmatrix} 1 & 0 & 0 \\ 0 & \cos \theta_A & -\sin \theta_A \\ 0 & \sin \theta_A & \cos \theta_A \end{pmatrix}, R_Y = \begin{pmatrix} \cos \theta_B & 0 & \sin \theta_B \\ 0 & 1 & 0 \\ -\sin \theta_B & 0 & \cos \theta_B \end{pmatrix} \tag{4}$$

where \$\theta_A, \theta_B\$ represents the rotation angle about X-axis and Y-axis, respectively.

The position of platform center is \$\overline{OP_0} = \overline{OT} - \overline{P_0T}\$. This also varies with the tool posture as

$$\overline{P_0T} = R_X R_Y \{ 0 \ 0 \ t \}^T \tag{5}$$

where \$t\$ is a length of tool, and \$P_0\$ is a center of the platform.

Thus, Eqs. (1)–(5) gives the relation between tool position \$\overline{OT}\$, tool posture \$\overline{P_0T}\$ and lengths of arms \$l_k = |\overline{B_kP_k}|\$.

Figure 3 shows examples of two tool postures \$\theta_B = \pm 25^\circ\$ for a machining position \$(X, Y) = (-150, 0)\$ on the flat surface of workpiece, and the arm lengths which were calculated by Eqs. (1)–(5). These milling processes indicate that the contact between cutting tool and workpiece is constant to get the same conditions, except the direction of tool posture. In this machine, each length of arm affects to the posture of cutting tool. As shown in those figures, each length

of arms \$l_k\$ is not same for different tool posture, even with the same position. For negative tool posture \$\theta_B\$, the total length of arm was larger than positive tool posture.

Figure 4 shows the calculated length of arms during the tool travels a cutting path which was employed in the milling test. Figure 4a presents examples for the path parallel with X-axis (\$X = -110\$ to \$-190\$) and a constant tool postures of \$\theta_B = \pm 25^\circ\$, while Fig. 4b gives examples for the path parallel with Y-axis (\$Y = -40\$ to \$40\$) and \$\theta_A = \pm 25^\circ\$. As can be seen in Fig. 4a, the influence of position on each arm length is not same; the lengths of arm \$l_2, l_3, l_4\$, and \$l_5\$ increase with feeding direction \$V_X\$, but \$l_1\$ and \$l_6\$ are slightly decreased. The total length of arm increases with the tool position \$X\$ for \$\theta_B = -25^\circ\$. Besides, the total length exhibits constant for posture \$\theta_B = +25^\circ\$. Thus, the dimensional structure changes with the tool travel. In Fig. 4b for the path parallel with Y-axis, however, the total length is free from large influence of the tool position \$Y\$ and posture \$\theta_A\$.

2.2 Modal Parameters and Hammering Test

The intermittent cutting generally generates periodic forces exciting the cutting system, and another vibration source is regenerative effect [17, 18]. Dynamics of cutting system is modelled as shown in Fig. 5, which is described with modal parameters: mass \$M\$, damper \$C\$, and stiffness \$K\$. We can derive the dynamic compliance of system, which is a ratio of displacement \$Q(\omega)\$ to force \$F(\omega)\$ as follows [19, 20]:

$$G(\omega) = \frac{Q(\omega)}{F(\omega)} = \frac{1}{(-\omega^2 M + i\omega C + K)} \tag{6}$$

Above is a transfer function of the system whose input and output are the force and the displacement, respectively. For multi degrees of freedom, the transfer function matrix \$[G(\omega)]\$ can be described as follows,

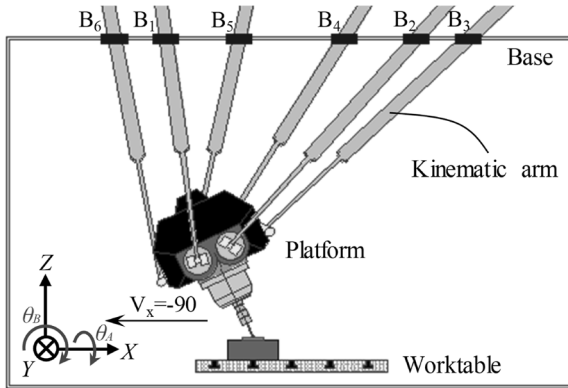
$$[G(\omega)] = \begin{bmatrix} G_{xx}(\omega) & G_{xy}(\omega) & G_{xz}(\omega) \\ G_{yx}(\omega) & G_{yy}(\omega) & G_{yz}(\omega) \\ G_{zx}(\omega) & G_{zy}(\omega) & G_{zz}(\omega) \end{bmatrix} \tag{7}$$

where \$G_{yx}(\omega)\$ represents the dynamic compliance in \$x\$ direction for the force in \$y\$ direction.

Hammering tests is commonly used to measure the modal parameters (\$M, C\$, and \$K\$) in transfer function \$G(\omega)\$ of structure, because it is difficult to determine them theoretically for actual cutting systems. For the PKM in this study, the tool posture and position are considered to vary the machinery stiffness \$K\$ which has significant effects on the structural dynamics.

So that, we investigated the machinery stiffness for different tool postures and position on the PKM by hammering test as shown in Fig. 6. We focused on the dynamic behavior of the tool-spindle systems, because the cutting

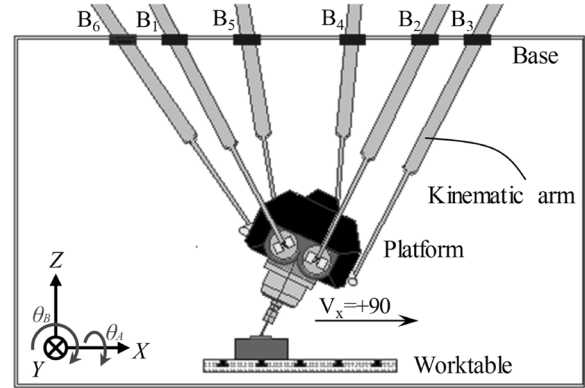
X	Y	θ_A	θ_B	V_X	V_Y
-150	0	0°	-25°	-90	-



Description	l_k (mm)
l_1 (B_1 to P_1)	875
l_2 (B_2 to P_2)	1,050
l_3 (B_3 to P_3)	1,029
l_4 (B_4 to P_4)	932
l_5 (B_5 to P_5)	999
l_6 (B_6 to P_6)	923
Total length of arm	5,808

(a) Negative tool posture ($\theta_A = 0^\circ, \theta_B = -25^\circ$)

X	Y	θ_A	θ_B	V_X	V_Y
-150	0	0°	+25°	+90	-



Description	l_k (mm)
l_1 (B_1 to P_1)	889
l_2 (B_2 to P_2)	962
l_3 (B_3 to P_3)	1,025
l_4 (B_4 to P_4)	980
l_5 (B_5 to P_5)	868
l_6 (B_6 to P_6)	842
Total length of arm	5,566

(b) Positive tool posture ($\theta_A = 0^\circ, \theta_B = +25^\circ$)

Fig. 3 Examples of arm lengths affected by tool posture (a negative tool posture, b positive tool posture)

tool system was considered as the flexible part in our experiment. Therefore, the carbide tool was hit by a hammer in x -, y -, and z -directions, and the response signals were measured by a three-axis accelerometer fixed on the tool tip. Then, the signals were acquired with sampling rate of 50 kHz by a data storage system. In this study, the hammering tests were conducted for four tool postures at several positions A, B, C, and D shown in Fig. 7. It should be noted that arrangements of the tool positions and the base joints are symmetric with respect to Y -axis, both. But, the arrangement of base joints is asymmetric with respect to X -axis, while that of tool positions is symmetric.

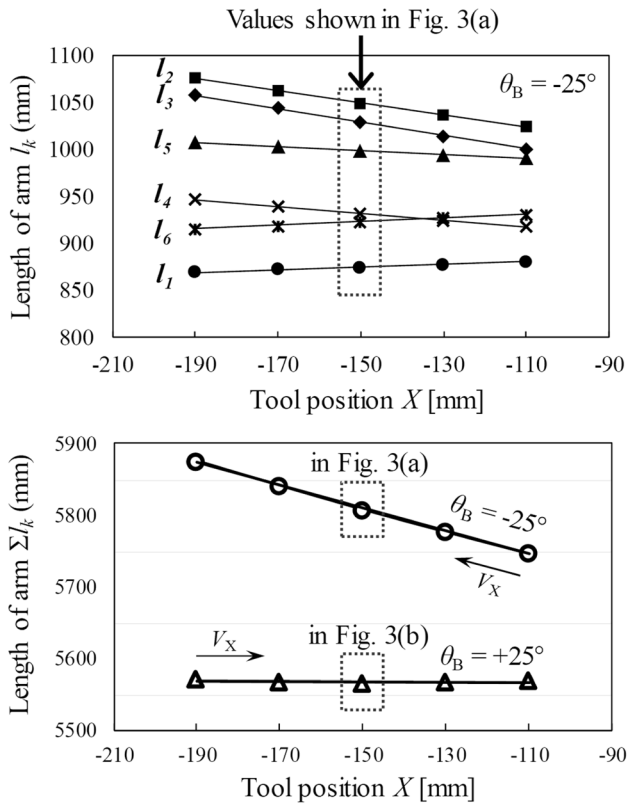
Figure 8 shows an example of frequency response function (FRF), which was measured by combining the Fourier spectra of the impulse force and the displacement both [21]. By using these curves, the modal parameters can be estimated. The real part of FRF has two highest peaks at specific frequencies **a** and **b**. Besides, the imaginary part of FRF has the highest peak value **c**, which is identified for natural frequency f_n . According to these frequencies:

a, **b**, **c** and amplitude of **c**, the modal parameters can be estimated [22].

2.3 Milling Tests

The slot milling was conducted under dry cutting on flat work surface using a ball-end mill to investigate the machining stability influenced by tool posture and position. The tool postures and positions were similar to ones in the hammering tests shown in Fig. 7. The workpieces used in these tests were flat plates of stainless steel ($130 \times 80 \times 10$ mm, JIS SUS 304), which is widely used in industries [23]. The workpiece was tightly fixed on the table of machine tool, therefore it can be assumed as a rigid body. The cutting tools used were ball end-mills with two flutes (Mitsubishi Hitachi Epoch Panacea Ball HGOB2060-PN), whose specifications are given in Table 1.

Figure 9 shows an experimental setup in ball-end milling under the conditions given in Table 2. Then, the



(a) Influence of tool position X on cutting path

(b) Influence of tool position Y on cutting path

Fig. 4 Change in arm length for tool posture $\theta_B = \pm 25^\circ$ and $\theta_A = \pm 25^\circ$ with tool traveling path near position $(X, Y) = (-150, 0)$

cutting force and vibration were measured by a three-axis dynamometer and an accelerometer mounted on the workpiece. The measured signals were stored by a data acquisition system (Yokogawa SL-1400) with a sampling rate of 50 kHz, and these signals were analyzed by FFT and HHT. Furthermore, the machining errors also were evaluated, such as: surface roughness and width of slot.

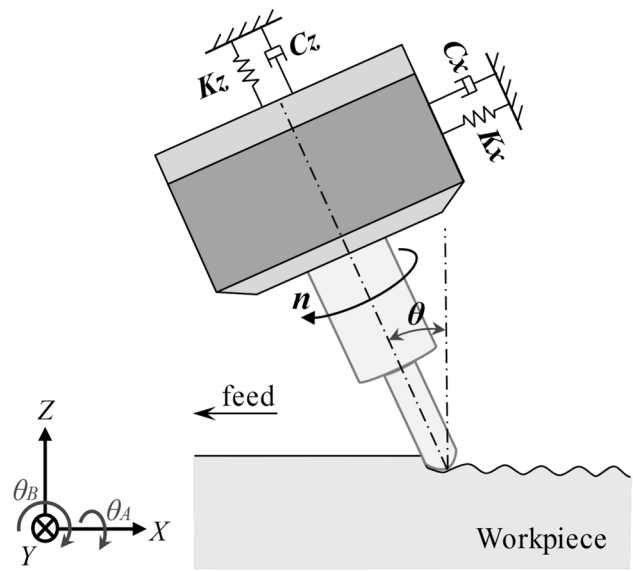


Fig. 5 Dynamic model of ball-end milling with inclination

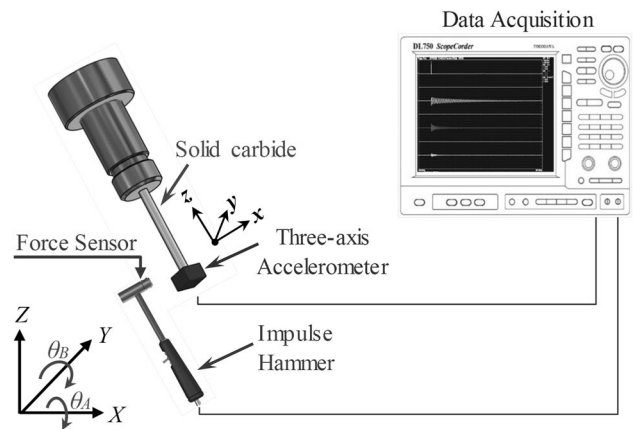
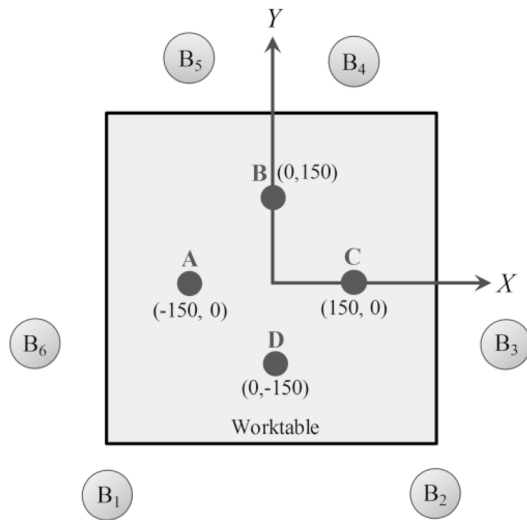


Fig. 6 Experimental setup for hammering tests

3 Results and Discussion

3.1 Machinery Stiffness with Considering the Length of Arm

Figure 10 summarizes influence of the total length of arms to the machinery stiffness and the natural frequency for four tool postures at several positions. As shown in the figure, the machinery stiffness K decreased with the total length of arms for any tool position, while the natural frequency f_n exhibited no significant change. For example, the stiffness decreased by 40% with the increase of length by 4% under the conditions shown in Fig. 10a–c. We can also summarize the influence of total length as: the highest



Four tool postures for any position (Example: position A)

No.	X	Y	θ_A	θ_B	V_X	V_Y
1	-150	0	0°	-25°	-90	-
2	-150	0	0°	+25°	+90	-
3	-150	0	-25°	0°	-	+90
4	-150	0	+25°	0°	-	-90

Fig. 7 Setup of four tool postures at several positions

stiffness was obtained when tool inclines to the inside of table as shown in Fig. 3b. But, the influence of length was not uniform at all positions; the stiffness highly depended on the length at A, B, and C, while the stiffness was saturated at D. Comparing three directions of stiffness for any position, z-direction had the highest stiffness, and the next highest stiffness was obtained in y-direction. This would be a characteristic peculiar to the machine tools used in this study.

3.2 Machining Stability in Milling Tests

Figure 11 gives examples of the acceleration signals and the frequency spectra, which were measured in milling tests with four tool postures at position A (X, Y) = (-150, 0). As shown in the figure, the machining stability varied with the tool posture; the amplitude of vibrating signal was largest with posture $\theta_B = -25^\circ$ (see Fig. 11a), while it was smallest with posture $\theta_B = +25^\circ$ (see Fig. 11b) among four postures. This trend corresponds reasonably well with the influence of posture to stiffness shown in Fig. 10a.

In this study, FFT analysis was conducted to identify distinctive frequencies in the measured signals, such as a tooth-passing frequency f_T or another distinctive frequency [24, 25]. Figure 11 also shows the frequency spectra of acceleration signal for four tool postures at position A (X, Y) = (-150,

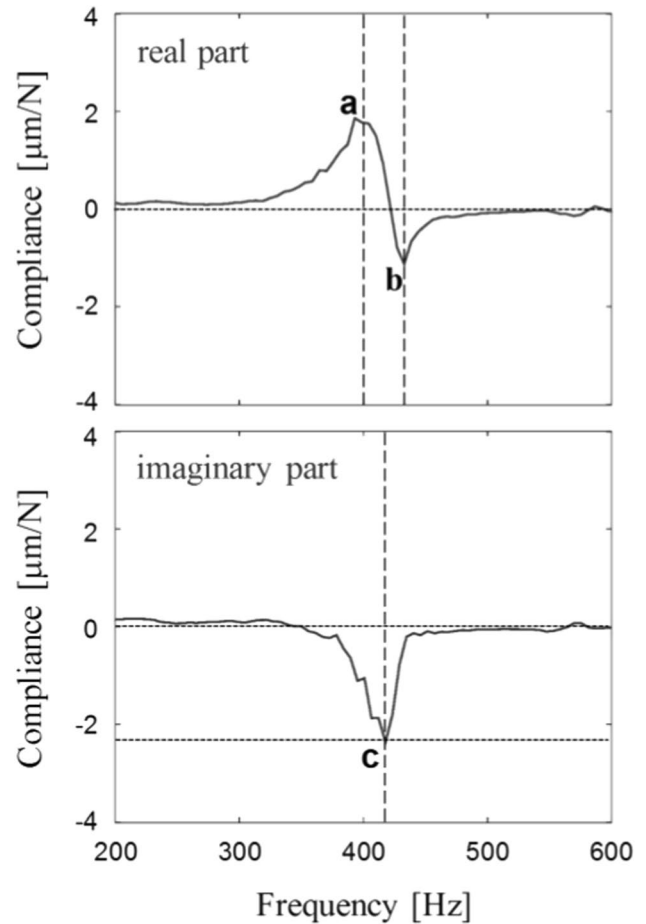


Fig. 8 Example of frequency response function $G(\omega)$ measured by impulse response method

Table 1 Specification of cutting tool

Tool diameter D (mm)	6	Material	Carbide
Number of flutes N_f	2	Coating	TiAlN
Helix angle (deg)	30	Tool length (mm)	90
Flute length (mm)	12	Overhang (mm)	60

0). The tooth-passing frequency is $f_T = N_f(n/60) = 30$ Hz under the experimental conditions. According to Fig. 11, the peaks appeared around frequency of chatter f_c , which is commonly near with the natural frequency of system f_n . Comparing the results in the figure, the frequencies were same for any tool postures. However, the peaks in frequency spectrum became highest for $\theta_B = -25^\circ$, while that for $\theta_B = +25^\circ$ was the smallest among four postures. Therefore, the maximum difference of peak-height was 250% between (a) $\theta_B = -25^\circ$ and (b) $\theta_B = +25^\circ$.

We could not observe the peak of tooth-passing frequency f_T in Fig. 11, this is because that the accelerometer has low sensitivity in lower frequency range [6]. So that,

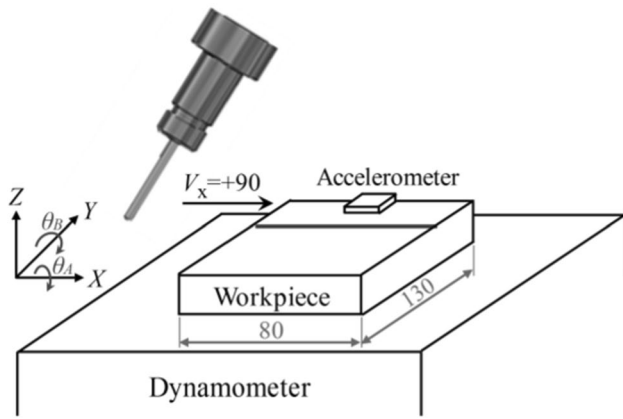


Fig. 9 Experimental setup in milling tests

Table 2 Cutting conditions for milling tests

Spindle rotation n (min^{-1})	900
Feed per tooth f (mm/tooth)	0.05
Feeding speed V (mm/min)	90
Depth of slot a (mm)	0.30
Tool posture θ (deg)	± 25

we also measured cutting forces to analyze the vibration. Figure 12 shows the dynamic and static of cutting force signals from dynamometer in milling operation at position A (X, Y) = (-150, 0). In the figure, the green color denotes the measured signal of dynamic forces, while the red color denotes the static force signal obtained through the low-pass filter with a cut-off frequency of 200 Hz. For tool posture $\theta_B = -25^\circ$ (in Fig. 12a), the static forces were constant during milling process, but the dynamic forces fluctuated and gradually increased during the milling. This is because of the change in machinery stiffness affected by the length of arms, which increased along the cutting path as shown in Fig. 4a. Besides, for tool posture $\theta_B = +25^\circ$ (in Fig. 12b), the static and dynamic forces were constant during milling process. This is because that the length of arm exhibited constant as shown in Fig. 4a.

In order to analyze the instantaneous changes in frequency component during milling process, the time–frequency spectra are also presented in Fig. 12. These results were obtained by Hilbert–Huang transform (HHT), which is a powerful signal processing method for nonlinear and nonstationary signals [26, 27]. In those spectra, the power of frequency component is indicated as a color map. And

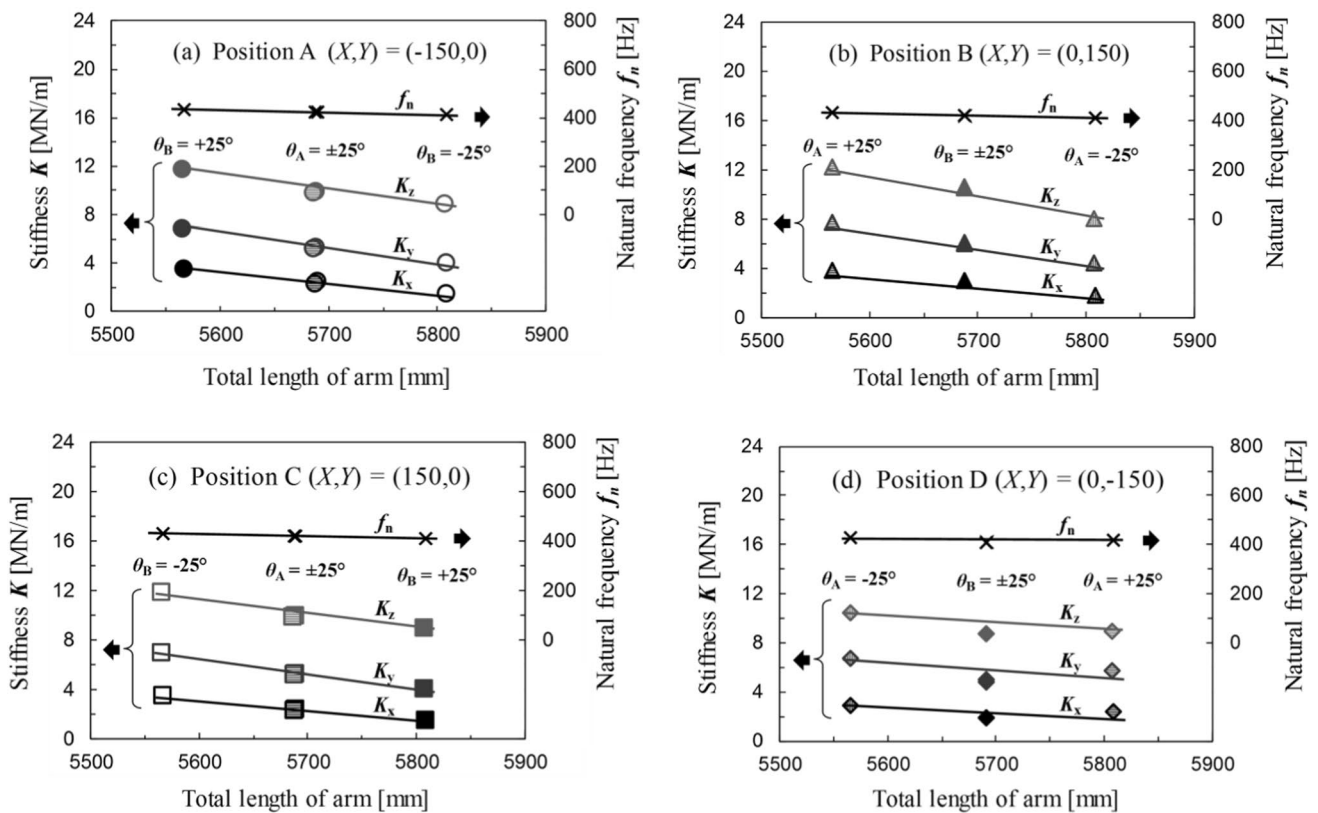


Fig. 10 Relationship between machinery stiffness with total length of arm for four tool postures at several positions

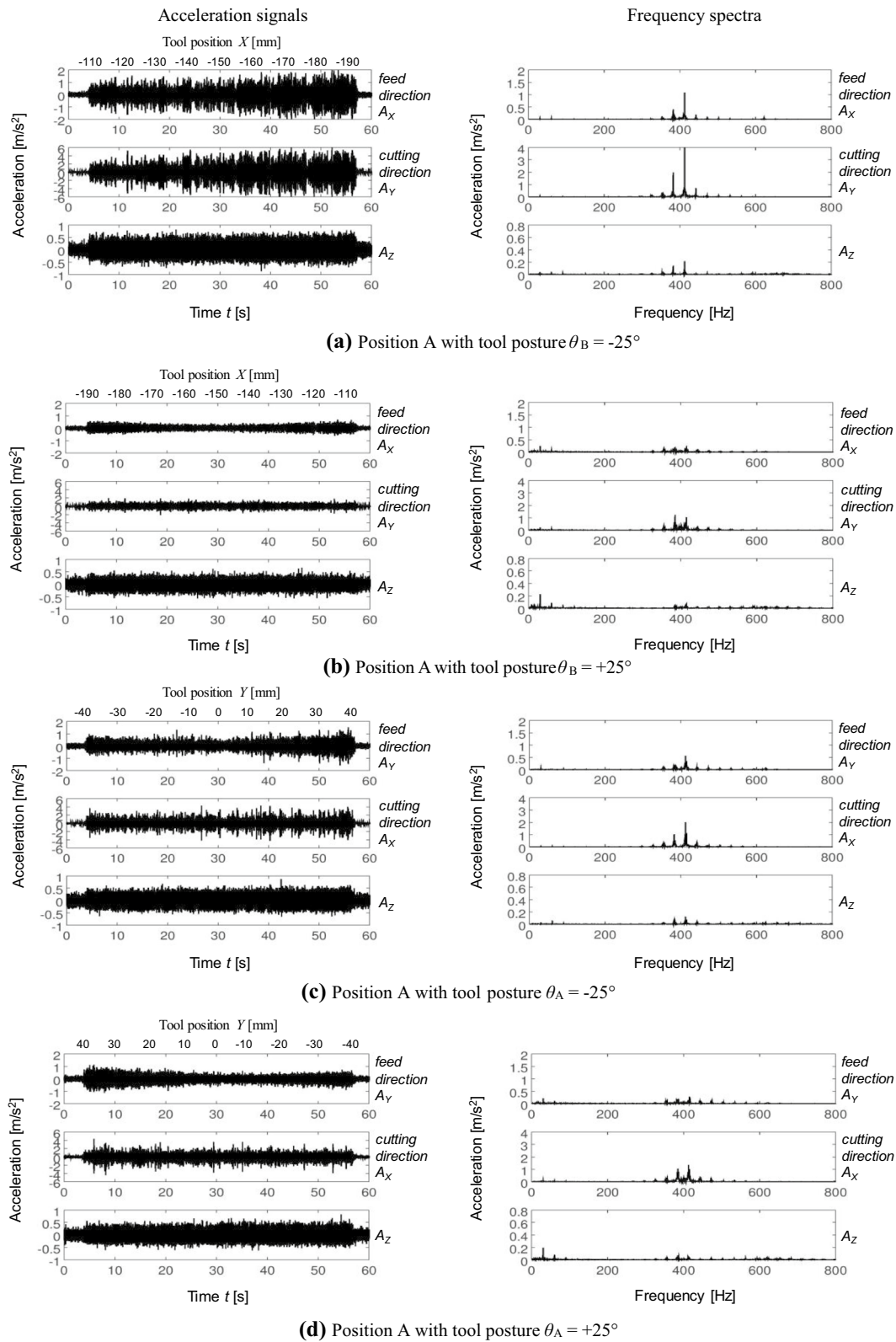


Fig. 11 Acceleration signals and frequency spectra in milling with four tool postures at position A $(X, Y) = (-150, 0)$

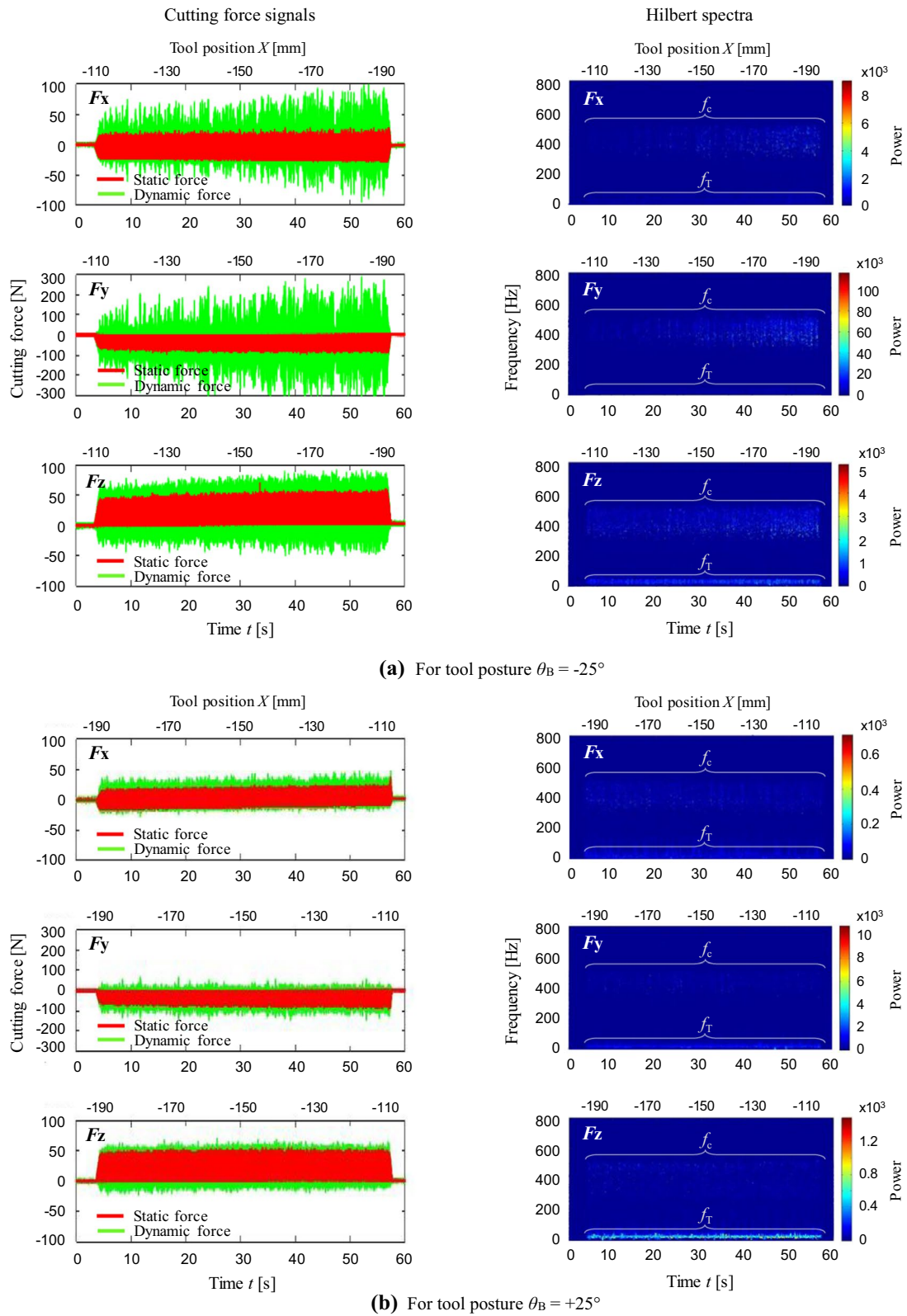


Fig. 12 Dynamic and static cutting forces for position A $(X, Y) = (-150, 0)$ with different tool posture θ_B and its Hilbert spectra

here, both the tooth-passing frequency f_T and the chatter frequency f_c are observed for any tool posture.

For tool posture $\theta_B = -25^\circ$ (in Fig. 12a), the power of f_T exhibit constant, but the power of f_c increased during the milling period, especially for signals F_x and F_y . And, the power level of chatter frequency f_c is slightly higher than that of tooth-passing frequency f_T . As shown in the figures, the power of f_c increased by 150% during the tool traveled only 80 mm in the milling operation. Besides, for tool posture $\theta_B = +25^\circ$ (in Fig. 12b), both frequencies exhibit constant over the milling period, and the power of f_c is lower than that of f_T .

The machining stability at position C exhibited same behavior as ones at position A (Figs. 11 and 12), because the structure of machine tool is symmetric with respect to Y -axis. Therefore, position B and D are discussed here. According to Fig. 10, the machinery stiffness is not similar at positions B and D, this is because the arrangement of

base joints is asymmetric with respect to X -axis (see Fig. 7). Hence, the stabilities in both positions were investigated. Figure 13 compares the acceleration signals for same tool posture $\theta_B = -25^\circ$ at positions B and D. As shown in the figure, the vibration at position D was larger than that at position B, and the frequency spectra also show the higher peaks at position D. Thus, an asymmetry of structure causes the difference in stability even for same tool postures.

3.3 Machining Errors in Milling Tests

Influence of tool posture and position on the machining errors were also investigated such as surface roughness or width of slot [28, 29]. Figure 14 shows the arithmetic roughness R_a (ISO 4287), which was measured at bottom of the slots machined at positions A-D with four postures. Measurement was repeated three times for the four points chosen on each slot, and the averaged values are shown here. In the

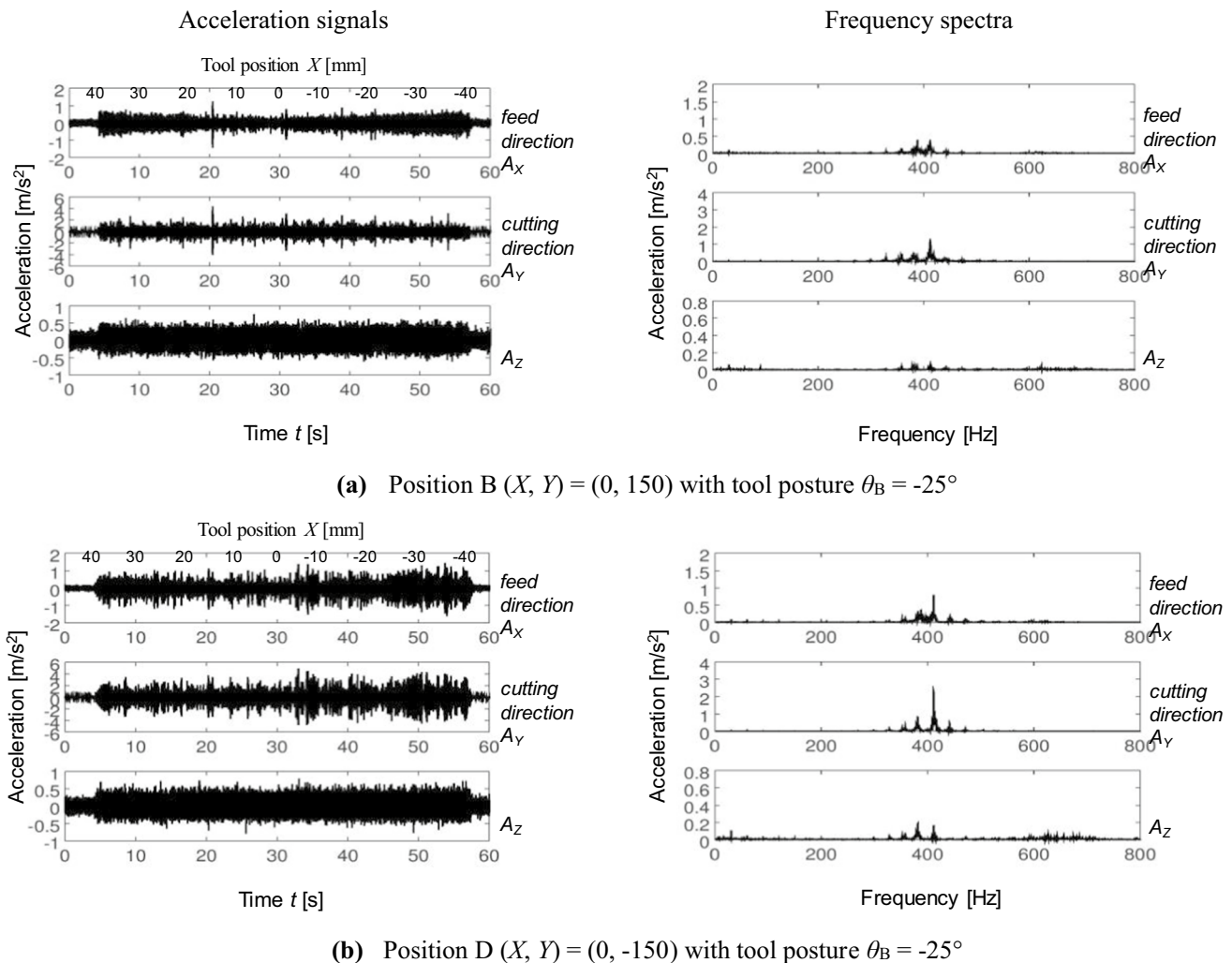


Fig. 13 Acceleration signals and frequency spectra in milling with constant tool posture for position B and D

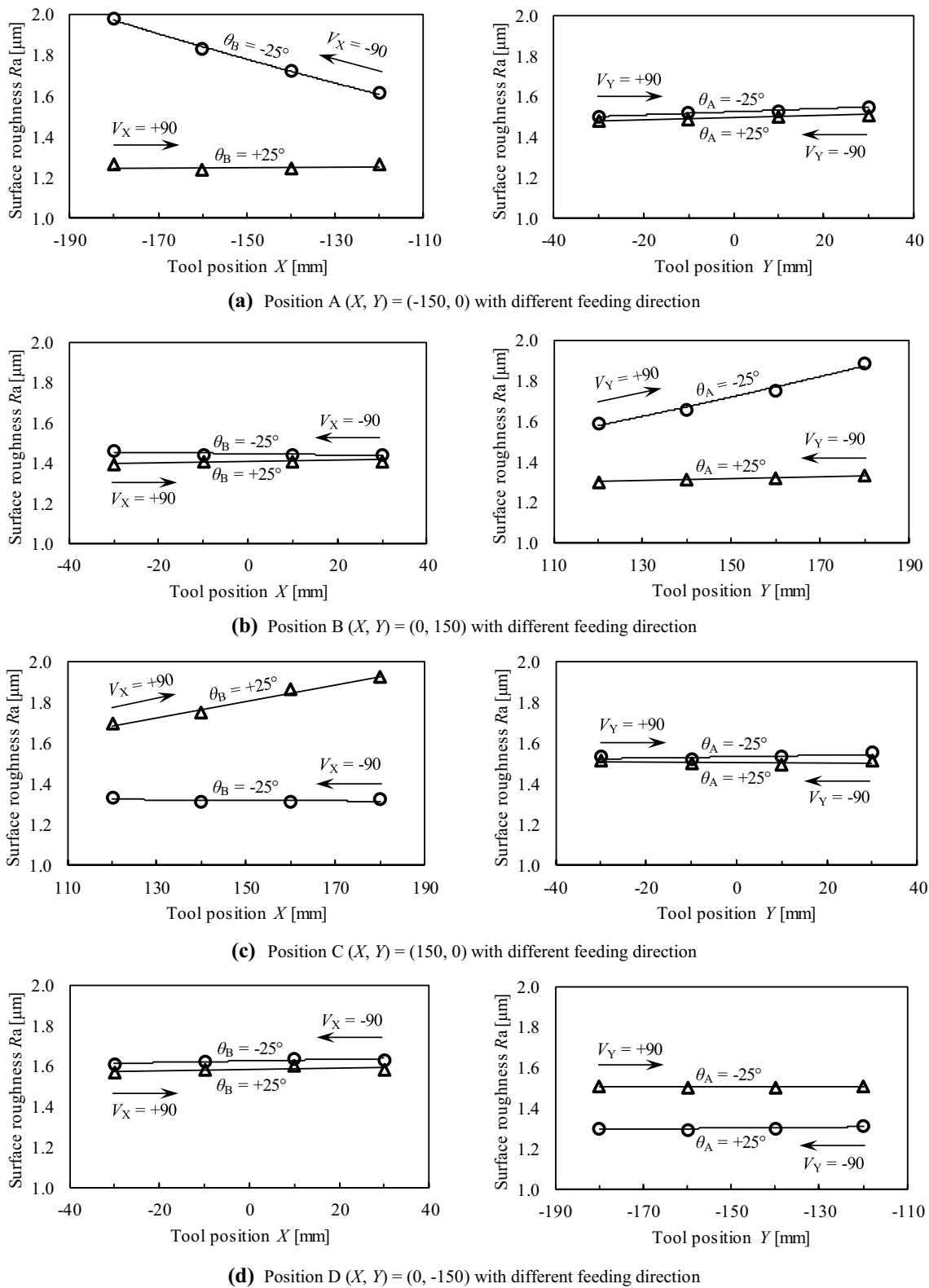
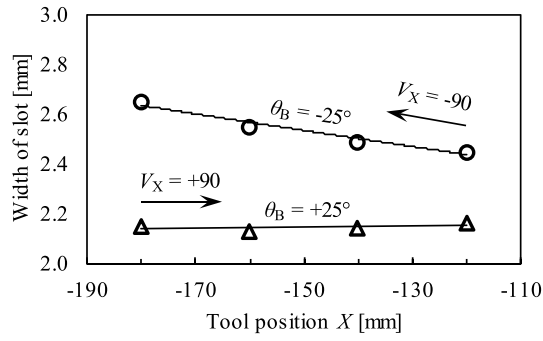
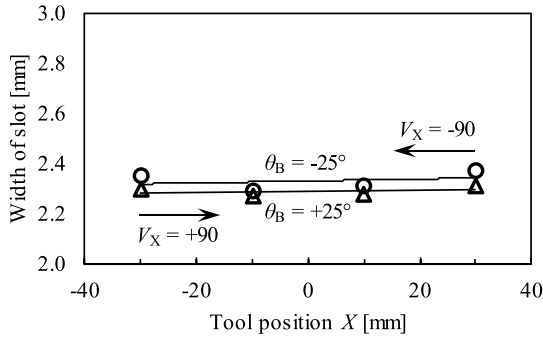
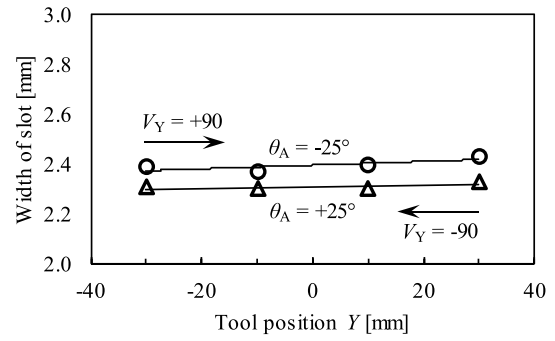


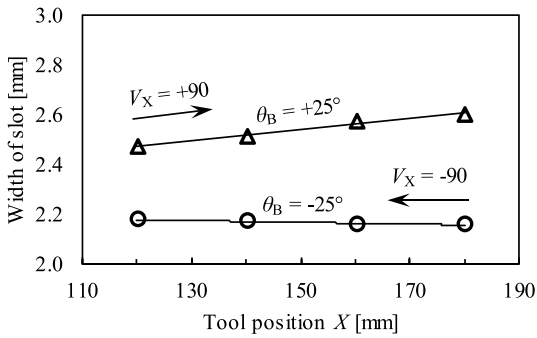
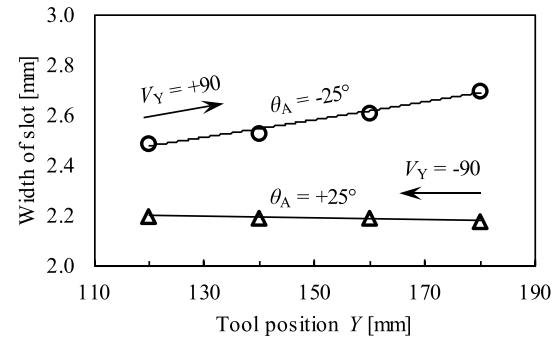
Fig. 14 Measured surface roughness at bottom of the slots machined at positions A to D with four tool postures



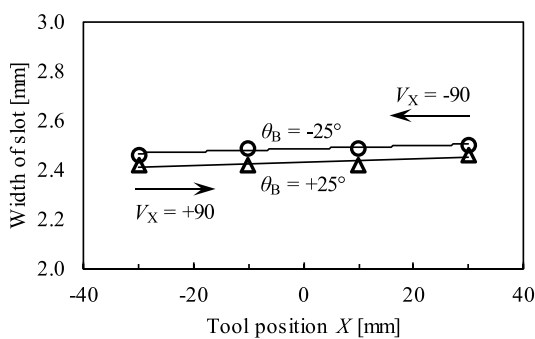
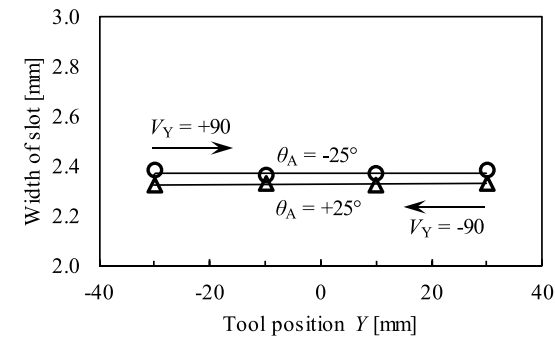
(a) Position A (X, Y) = (-150, 0) with different feeding direction



(b) Position B (X, Y) = (0, 150) with different feeding direction



(c) Position C (X, Y) = (150, 0) with different feeding direction



(d) Position D (X, Y) = (0, -150) with different feeding direction

Fig. 15 Measured width of slot machined at positions A to D with four tool postures

figure, arrows indicate the feeding directions in slot milling process. As can be seen, the feeding in X -direction affected the roughness at positions A and C, while the feeding in Y -direction exhibited no effect on the roughness. Besides, at positions B and D, the feeding in Y -direction affected. This is due to the influence of the change in arm length. For example, as shown in Fig. 4, the length depends on not position- Y but the position- X at tool position A (X, Y) = (-150, 0). Thus, we have to consider the geometric influence to decide the appropriate feeding direction for stable milling process on the PKMs. In our experiments, the maximum change in roughness was 0.4 μm during the tool position changed by 60 mm.

Figure 15 shows the measured width of slot machined under several conditions for the four points chosen on each slot. In slot milling, the slot width is affected by the vibration in cutting direction. For example, in the milling at position A with tool posture $\theta_B = -25^\circ$ (see Fig. 15a), the slot width increased as the tool position moved from $X = -110$ to $X = -190$ mm. This is similar to that the acceleration gradually increased with during the milling process shown in Fig. 11a. Furthermore, compared with Fig. 14, the conditions obviously had same influence on the slot width and the surface roughness both.

4 Conclusions

This paper demonstrates the machining stability influenced by tool posture and position in milling process on the parallel kinematic machine tool (PKM). The geometric structure was calculated, and the machinery stiffness was measured by impulse respond method. Then, the milling tests were conducted to analyze the machining stability. Following results emerged through this study:

1. Machinery stiffness of PKM receives an effect of total length of the arms supporting the spindle head. For example, the stiffness decreased by 40% with the increase of length by 4% under some conditions. And the higher stiffness was obtained when the tool inclined to the inside of worktable on the PKM.
2. The machining stability strongly depended on the tool posture and position during the milling process on PKM, which was similar to the dependency of stiffness of the system. The difference of peak-height was up to 250% between four postures in frequency spectra of acceleration signal.
3. Hilbert spectra presented the transition of power and frequency of vibration excited in the milling process where the dimensional structure continuously changed in. For example, the power of force signal increased by

150% during the tool traveled only 80 mm in the milling operation.

4. Surface quality and dimensional error depend on the machining stability which varies with tool position and posture in the slot milling process. The maximum change in roughness was 0.4 μm during the tool position changed by 60 mm. And the slot width showed similar trend as observed for the roughness.

Considering these conclusions, this study confirmed that the length of arm has dominant influence on the stability. In addition, it was clarified that the vibration can be reduced by selecting the appropriate posture and position of the tool.

Acknowledgements The first author acknowledges the scholarship support from Research & Innovation in Science & Technology Project (Riset-Pro) in Ministry of Research and Technology of the Republic of Indonesia.

References

1. Altintas, Y., & Lee, P. (1998). Mechanics and dynamics of ball end milling. *ASME*, *120*, 684–692.
2. Altintas, Y., Shamoto, E., Lee, P., & Budak, E. (1999). Analytical prediction of stability lobes in ball end milling. *ASME*, *121*, 586–592.
3. Shamoto, E., & Akazawa, K. (2009). Analytical prediction of chatter stability in ball end milling with tool inclination. *CIRP Annals—Manufacturing Technology*, *58*, 351–354.
4. Matsumura, T., Miyahara, Y., & Ono, T. (2008). Dynamic characteristics in the cutting operations with small diameter end mills. *Journal of Advance Mechanical Design, Systems, and Manufacturing*, *2*(4), 609–618.
5. Selmi, J., Costes, J. P., et al. (2013). *Spindle position influence on milling operation stability*. Bordeaux: Congres Francais de Mecanique.
6. Azka, M., Yamada, K., et al. (2020). Hilbert–Huang transform analysis of machining stability in ball-nose end-milling of curved surface. *International Journal of Automation Technology*, *14*(3), 500–511.
7. Tlustý, J., Ziegert, J. C., et al. (2000). A comparison of stiffness characteristics of serial and parallel machine tools. *Journal of Manufacturing Process*, *2*(1), 67–76.
8. Pandilov, Z., & Rall, K. (2006). Parallel kinematics machine tools: History, present, future. *Mechanical Engineering—Scientific Journal*, *25*(1), 1–46.
9. Rosyid, A., El-Khasawneh, B., & Alazzam, A. (2020). External kinematic calibration of hybrid kinematics machine utilizing lower-DOF planar parallel kinematics mechanisms. *International Journal of Precision Engineering and Manufacturing*, *21*, 995–1015.
10. Wiens, G. J., & Hardage, D. S. (2006). Structural dynamics and system identification of parallel kinematic machines. In *Proceedings of IDETC/CIE, ASME*.
11. Harib, K. H., Ullah, A. M. M., & Hammami, A. (2007). A hexapod-based machine tool with hybrid structure: Kinematic analysis and trajectory planning. *International Journal of Machine Tools and Manufacture*, *47*, 1426–1432.
12. Merlet, J. P. (2002). An initiative for the kinematics study of parallel manipulators. In *Proceedings of the workshop on fundamental*

issues and future research directions for parallel mechanisms and manipulators, Quebec, Canada, October 3–4.

13. Tunc, L. T., & Shaw, J. (2016). Investigation of the effects of Stewart platform-type industrial robot on stability of robotic milling. *International Journal Advance Manufacture Technology*. <https://doi.org/10.1007/s00170-016-8420-z>.
14. Li, Y., & Xu, Q. (2004). *Kinematics and stiffness analysis for a general 3-PRS spatial parallel mechanism*. Montreal, Canada: ROMANSY.
15. Lian, B., Sun, T., et al. (2015). Stiffness analysis and experiment of a novel 5-DoF parallel kinematic machine considering gravitational effects. *International Journal of Machine Tools and Manufacture*, 95, 82–96.
16. Xu, P., Li, B., Cheung, C. F., & Zhang, J. F. (2017). Stiffness modeling and optimization of a 3-DOF parallel robot in a serial-parallel polishing machine. *International Journal of Precision Engineering and Manufacturing*, 18, 497–507.
17. Altintas, Y. (2001). Analytical prediction of three-dimensional chatter stability in milling. *JSME International Journal*, 44(3), 717–723.
18. Chang, W. Y., Chen, C. C., & Wu, S. J. (2019). Chatter analysis and stability prediction of milling tool based on zero-order and envelope methods for real-time monitoring and compensation. *International Journal of Precision Engineering and Manufacturing*, 20, 693–700.
19. Stephenson, D. A., & Agapiou, J. S. (2006). *Metal cutting theory and practice* (2nd ed., p. 380, 620). Boca Raton: CRC Press.
20. Rubio, L., De la Sen, M., et al. (2019). Analysis of discrete time schemes for milling forces control under fractional order holds. *International Journal of Precision Engineering and Manufacturing*, 14(5), 735–744.
21. Altintas, Y. (2012). *Manufacturing automation: metal cutting mechanics, machine tool vibrations, and CNC design* (2nd ed., pp. 92–98). Cambridge: Cambridge University Press.
22. Li, Z., Wang, Z., & Shi, X. (2017). Fast prediction of chatter stability lobe diagram for milling process using frequency response function or modal parameters. *International Journal of Advanced Manufacturing Technology*, 89, 2603–2612.
23. Xu, Z., Ming, L., Dinghua, Z., & Wanzhu, L. (2016). Cutting force prediction in four-axis milling of curved surfaces with bull-nose end mill. In *9th international conference on digital enterprise technology—DET* (vol. 56, pp. 100–104).
24. Altintas, Y., Stepan, G., Merdol, D., & Dombovari, Z. (2008). Chatter stability of milling in frequency and discrete time domain. *CIRP Journal of Manufacturing Science and Technology*, 1, 35–44.
25. Yoo, Y. J. (2019). Fault detection of induction motor using fast fourier transform with feature selection via principal component analysis. *International Journal of Precision Engineering and Manufacturing*, 20, 1543–1552.
26. Huang, N. E., & Shen, S. (2005). *Hilbert–Huang transform and its applications*. Singapore: World Scientific Publishing.
27. Susanto, A., Liu, C. H., Yamada, K., et al. (2018). Application of Hilbert–Huang transform for vibration signal analysis in end-milling. *Precision Engineering*, 53, 263–277.
28. You, S. H., Lee, J. H., & Hoon, S. (2019). A study on cutting characteristics in turning operations of titanium alloy used in automobile. *International Journal of Precision Engineering and Manufacturing*, 20, 209–216.
29. Muhammad, I., Khatoon, T., Ullah, S. M., & Ko, T. J. (2018). Development of empirical model for bio machining to improve machinability and surface roughness of polycrystalline copper.

International Journal of Precision Engineering and Manufacturing-Green Technology, 5, 201–209.

Publisher's Note Springer Nature remains neutral with regard to jurisdictional claims in published maps and institutional affiliations.



Muizuddin Azka Doctoral Student in the Department of Mechanical System Engineering, Hiroshima University, Japan. His research interest is complex surface machining, computer-aided manufacturing and signal processing. E-mail: muizuddin.azka@gmail.com.



Keiji Yamada Professor in the Department of Mechanical System Engineering, Hiroshima University, Japan. His research interest is machining stability, laser material processing and laser assisted machining. E-mail: keiji@hiroshima-u.ac.jp.



Mahfudz Al Huda of Machinery Industry (PTIP), Agency for Assessment and Application Technology (BPPT), Indonesia. His research interest is complex surface machining, non-destructive testing and sensing technology. E-mail: mahfudz.al@bppt.go.id.



Ryutaro Tanaka Associate professor in the Department of Mechanical System Engineering, Hiroshima University, Japan. His research interest is cutting temperature, machining of difficult-to-cut materials and tribology in metal cutting. E-mail: ryu-tanaka@hiroshima-u.ac.jp.



Katsuhiko Sekiya Assistant professor in the Department of Mechanical System Engineering, Hiroshima University, Japan. His research interest is machining of difficult-to-cut materials, coating for cutting tools and adhesion on cutting tool surface. E-mail: sekiya@hiroshima-u.ac.jp.